

Pretrained-Guided Conditional Diffusion Models for Microbiome Data Analysis

Xinyuan Shi^{1,†}, Fangfang Zhu^{2,†} and Wenwen Min^{1,*} 

¹School of Information Science and Engineering, Yunnan University, Kunming 650091, Yunnan, China

²College of Nursing Health Sciences, Yunnan Open University, 650599, Kunming, China

Abstract—Emerging evidence indicates that human cancers are intricately linked to human microbiomes, forming an inseparable connection. However, due to limited sample sizes and significant data loss during collection for various reasons, some machine learning methods have been proposed to address the issue of missing data. These methods have not fully utilized the known clinical information of patients to enhance the accuracy of data imputation. Therefore, we introduce mbVDiT, a novel pre-trained conditional diffusion model for microbiome data imputation and denoising, which uses the unmasked data and patient metadata as conditional guidance for imputing missing values. It is also uses VAE to integrate the the other public microbiome datasets to enhance model performance. The results on the microbiome datasets from three different cancer types demonstrate the performance of our methods in comparison with existing methods. Source code and all public datasets used in this paper are available at Github (<https://github.com/wenwenmin/mbVDiT>) and Zenodo (<https://zenodo.org/records/13254073>).

Index Terms—Microbiome data; Imputation; Diffusion model; Transformer; DiT

I. INTRODUCTION

Cancer is commonly regarded as a complex human genomic disease [1, 2]. With ongoing research, it has been discovered that the microbiome contributes significantly to certain types of cancer [3, 4]. Moreover, unique microbial features have been found within and between tissues and blood of most major types of cancer. These studies reveal the potential of microbiomes as tools for cancer diagnosis or treatment. The acquisition of microbiome data primarily relies on two sequencing technologies: the 16S ribosomal RNA (rRNA) amplicon sequencing and the shotgun metagenomic sequencing. The 16S rRNA amplicon sequencing technique quantifies 16S rRNAs, enabling the identification and differentiation of microbes [5]. Shotgun metagenomic sequencing, also referred to as whole-genome sequencing (WGS), involves sequencing all DNA present in a microbiome sample, capturing entire genomes of microbial species as well as host DNA [6, 7].

A key challenge with microbiome data is the presence of numerous zero values (high sparsity), which is a common issue in both major sequencing methods [8], these zero values may arise due to sampling techniques or other factors leading to data gaps. The high sparsity characteristic of microbiome data results in poor performance for down analysis. Additionally,

the small sample size and lack of labels in microbiome data are significant factors that hinder the development of deep learning.

Imputation is a widely used technique to recover missing data and facilitate data analysis. In recent years, some methods have been based on GANs (Generative Adversarial Networks) and autoencoders. GANs have become popular in recent years as a method for generating new data through adversarial learning, producing data that conforms to the distribution of real data [9, 10]. Additionally, self-supervised deep learning methods and consistency models are applied in related areas [11, 12]. Similarly, autoencoder-based deep models, with their probabilistic foundations and capability to manage intricate distributions, excel at capturing the underlying representation of the data, rendering them essential for data imputation. These imputation methods have already achieved success in many fields, e.g., image and speech reconstruction [13], imputation of unmeasured epigenomics datasets [14], and imputation of gene expression recovery in single-cell RNA-sequencing (scRNA-seq) data [15–18]. However, existing methods have not fully utilized clinical information from patients to improve the imputation performance of the model. This results in wastage of data and missed opportunities to uncover potential data insights.

As generative deep models continue to advance, diffusion models are becoming increasingly popular and have been applied in various fields [19–22]. Starting from the initial denoising diffusion probabilistic models (DDPM) [23], the diffusion models have gradually evolved into score-based diffusion models [24] and are steadily maturing. Meanwhile, the integration of diffusion models with Transformer has provided researchers with more possibilities to fuse diverse information [25].

To address the challenges in this field, we introduce a novel method, mbVDiT for microbiome data imputation. Our approach primarily combines the excellent capabilities of variational autoencoders (VAE) in learning latent distributions and diffusion models in generating new data that conforms to the real data distribution. To address the issue of unlabeled microbiome data, we drew inspiration from recent research in the field [26, 27]. We masked a portion of the original data, which remained invisible throughout the entire modeling process and served as labels for evaluating the imputation performance after filling. After the masked data is encoded

[†]These authors contributed equally to this work.

*Corresponding author: minwenwen@ynu.edu.cn

into the latent space by the VAE encoder, we re-mask the latent space and employ a conditional score-based diffusion model for training the denoising network. Our goal is to reconstruct a cancer microbiome data matrix by integrating various types of metadata information from patients and handling the label-less nature of the data. Make the most of existing conditions to improve the accuracy of imputed data while preserving the inherent characteristics and distribution patterns of the data. The main contributions of our proposed method are:

- Through the application of pre-training strategy, we achieved common features across different cancer type datasets. Using data from other types of cancers has improved the model performance through cross-utilization caused by the limited number of samples in individual datasets.
- Using masking for self-supervised learning addresses the challenge of lacking labels in microbiome data.
- Using various types of metadata from cancer patients as conditions has improved the model performance.

II. PROPOSED METHODS

A. Overview of the proposed mbVDiT

We propose a conditional diffusion model, mbVDiT, for microbiome data imputation (Fig. 1). The model is able to perform accurate and stable imputation using the unmasked latent microbiome data and patient metadata.

B. mbVDiT model

1) *Mask strategy*: Due to the lack of labels in microbiome data, we employ self-supervised learning methods [26]. To assess the impact of different missing rates on model performance, we randomly mask 10%, 30% and 50% of the non-zero elements for each given data matrix and designate this masked portion as the test set for subsequent model computation and evaluation of performance metrics. Specifically, a mask matrix M is defined.

$$M = \begin{cases} 1, & \text{if } x_{ij} \text{ is masked} \\ 0, & \text{otherwise} \end{cases} \quad (1)$$

The mask matrix has the same dimensions as the input data, where $M \in R^{n \times d}$, x_{ij} represents the masked data. After masking, the final matrix $Y \odot M$ serves as the input for mbVDiT.

2) *Pre-training VAE*: The VAE model consists of an encoder and a decoder, maintaining consistency in both structure and functionality with the traditional model. Our main purpose in employing the VAE model is to capture the latent distribution and representation of data features from other cancer type datasets.

Specifically, we pre-train using four different types of cancer datasets and transfer the resulting pre-trained parameters to the VAE module of mbVDiT. After that, we train mbVDiT using a single dataset. It is important to note that this individual dataset is not included in the four pre-training datasets.

Formally, given input data X , $X \in R^{n \times d}$, representing a set of n samples with d features. the encoder maps the input to a

potential distribution, which contains two parameters, variance μ_i and mean σ_i^2 :

$$[\mu_i, \sigma_i^2] = \text{Encoder}(X_i) \quad (2)$$

where i denotes the microbial data features of a sample.

Then the decoder obtains a sample Z , $Z \sim \mathcal{N}(\mu_i, \sigma_i^2)$, from this latent distribution and completes the reconstruction of the data based on this sample:

$$\hat{X}_i = \text{Decoder}(Z) \quad (3)$$

3) *VAE-encoder in mbVDiT*: When the number of features exceeds the number of samples, a potential issue known as the curse of dimensionality may arise, which could lead to overfitting during model training and result in decreased model performance. Therefore, we introduce a VAE encoder to reduce the dimensionality of the data and train the model in the latent space containing the underlying distribution of the data. It is worth noting that the VAE module in this model is pretrained, including encoder and decoder.

Specifically, given a masked data X , it is mapped to a latent space H containing the underlying distribution of the data through the VAE encoder. By employing a fully connected layer, the encoder is denoted as f_θ^{en} . This can be formulated as:

$$H = f_\theta^{en}(X) \quad (4)$$

where $H \in R^{n \times l}$, n represents the number of samples and l represents the dimensionality of the latent space. This latent representation will be used for training the diffusion model.

4) *Conditional score-based diffusion model for posterior estimation*: In order to gain a deeper understanding of the diffusion model, we carefully studied the classic literature in the field of diffusion models [23, 28]. Follow the notations in denoising diffusion probabilistic models (DDPM). DDPMs are latent variable models consisting of two main processes: the forward process and the reverse process. The forward process is characterized by a Markov chain, outlined as follows:

$$q(x_{1:T} | x_0) = \prod_{t=1}^T q(x_t | x_{t-1}) \quad (5)$$

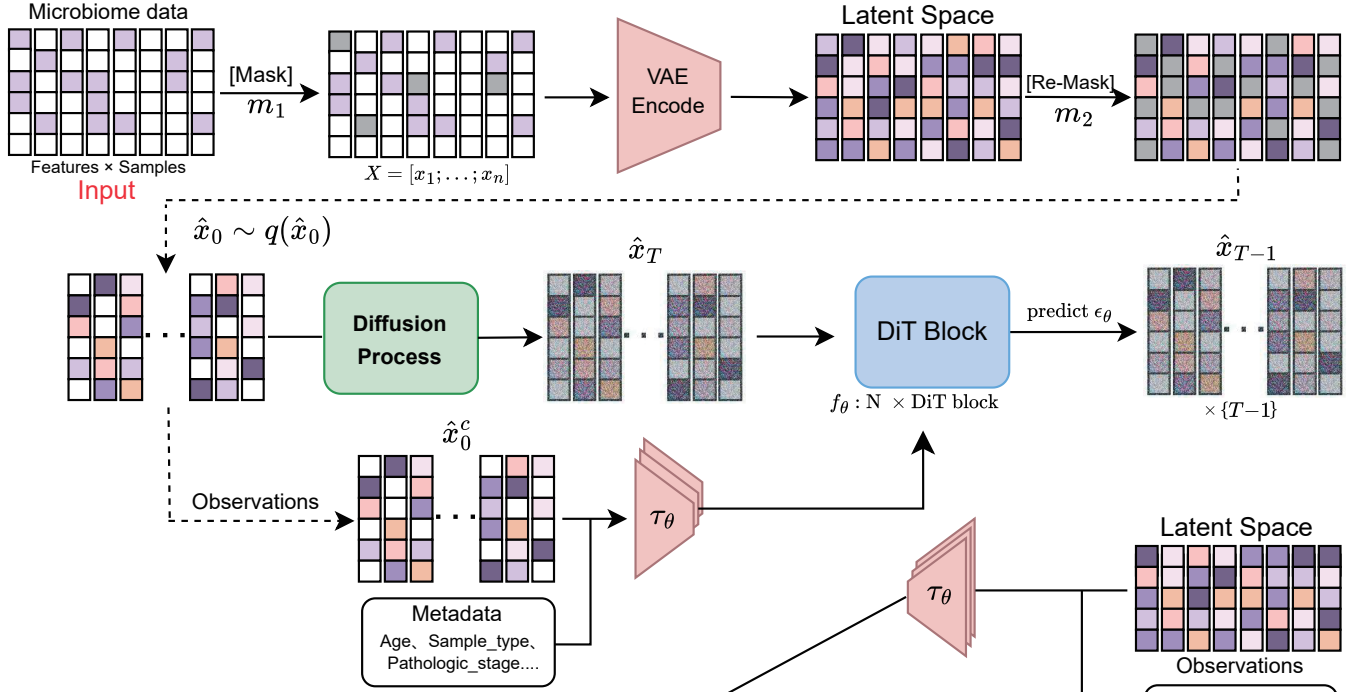
$$q(x_t | x_{t-1}) = \mathcal{N}(x_t; \sqrt{1 - \beta_t}x_{t-1}, \beta_t \mathbf{I})$$

where β_t is a small positive constant indicative of a noise level, $\{\beta_t\}_{t=1}^T \in (0, 1)$, and the numerical value increases with time. Through reparameterized sampling, we can obtain $q(x_t | x_0) = \mathcal{N}(x_t; \sqrt{\bar{\alpha}_t}x_0, (1 - \bar{\alpha}_t)\mathbf{I})$, where $\hat{\alpha}_t = 1 - \beta_t$ and α_t is the cumulative product $\bar{\alpha}_t = \prod_{i=1}^t \hat{\alpha}_i$. As a result, x_t can be expressed by the equation $x_t = \sqrt{\bar{\alpha}_t}x_0 + (1 - \bar{\alpha}_t)\epsilon$, with $\epsilon \sim \mathcal{N}(0, \mathbf{I})$. On the contrary, the reverse process is a denoising process, obtaining x_0 from x_t . This process can be defined as a Markov chain:

$$p_\theta(x_{0:T}) = p(x_T) \prod_{t=1}^T p_\theta(x_{t-1} | x_t) \quad (6)$$

$$x_T \sim \mathcal{N}(0, \mathbf{I})$$

A. Training process of mbVDiT



B. Inference process of mbVDiT

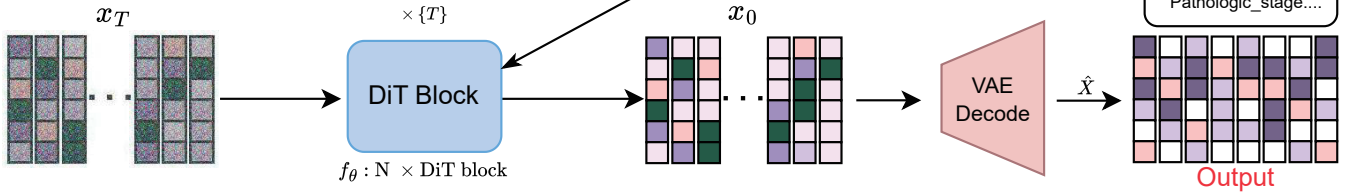


Fig. 1: The architecture of the proposed mbVDiT, where a VAE-based pre-trained model is used to integrate other public microbiome datasets to enhance model performance. (A) Training process: The latent space data \hat{x}_0 after masking is subjected to noise to obtain \hat{x}_T . Then, a denoising network f_θ is trained to predict the noise under the condition. (B) Inference process: The trained denoising network f_θ denoises the random noise x_T step-by-step under the guidance of the condition. The data after noise removal is then passed through a decoder, resulting in the predicted imputation for the microbiome data.

$$\begin{aligned}
 p_\theta(x_{t-1} | x_t) &= \mathcal{N}(x_{t-1}; \mu_\theta(x_t, t), \sigma_\theta^2(x_t, t)\mathbf{I}) \\
 \mu_\theta(x_t, t) &= \frac{1}{\bar{\alpha}_t} \left(x_t - \frac{\beta_t}{\sqrt{1 - \bar{\alpha}_t}} \epsilon_\theta(x_t, t) \right) \\
 \sigma_\theta(x_t, t) &= \beta_t^{1/2}
 \end{aligned} \tag{7}$$

where $\beta_t = \begin{cases} \frac{1 - \bar{\alpha}_{t-1}}{1 - \bar{\alpha}_t} \beta_1, & \text{for } t > 1 \\ \beta_1, & \text{for } t = 1 \end{cases}$ and $\epsilon_\theta(x_t, t)$ is a trainable denoising function. In our proposed approach, we utilize a score-based diffusion model, which distinguishes itself from the conventional DDPM primarily through distinct coefficients employed during the sampling phase.

5) *Conditioning mechanisms*: Our proposed method intends to estimate the entire dataset by leveraging the known data and patient metadata, such as pathological etc, as prior conditions. We aim to utilize the known data to complete missing value imputation, thereby reconstructing a complete representation of the dataset.

(1) **Observable data as the condition** We denote the observed data as x_0^o , $x_0^o = (E_{n,l} - m_2) \odot x_0$, where x_0 represents the latent representation at time step 0, m_2 is an element-wise indicator, $m_2 \in \{0, 1\}^{n \times l}$, where ones denote masked values and zeros denote observed values, and $E_{n,l}$ is all-ones matrix [21].

(2) **Patient metadata as the condition** Patient metadata includes both textual and floating-point data. For the integration of multiple types of conditions, we referred to some literature [29–31]. To pre-process y_i originating from diverse modalities, we introduce multiple domain-specific encoders (MLP) $\tau_{\theta,i}$ that map y_i to an intermediate representation, the dimensionality of this representation is the same as that of the feature dimension.

Overall, the conditions of the diffusion model are composed of observable data and metadata, which is then mapped to the intermediate layers of the backbone via a cross-attention layer

implementing.

$$C = \tau(x_0^c) + \tau_{\theta,i}(y_i) \quad (8)$$

where i represents the number of types of patient metadata and $\tau(\cdot)$ is a multilayer perceptron (MLP) that converts unmasked part of data as an input condition.

We define the imputation data for each time step as x_t^* . Hence, the conditional mechanisms within mbVDiT aim to estimate the probabilistic:

$$p_{\theta}(x_{t-1}^* | x_t^*, C) \quad (9)$$

To enhance the utilization of observed values as prior condition for the diffusion model in performing missing value imputation, we reformulate Equation (6) and Equation (7) as:

$$p_{\theta}(x_{0:T}^* | C) = p(x_T^*) \prod_{t=1}^T p_{\theta}(x_{t-1}^* | x_t^*, C) \quad (10)$$

$$x_T^* \sim \mathcal{N}(0, \mathbf{I})$$

$$p_{\theta}(x_{t-1}^* | x_t^*, C) = \mathcal{N}(x_{t-1}^*; \mu_{\theta}(x_t^*, t | C), \sigma_{\theta}^2(x_t^*, t | C) \mathbf{I}) \quad (11)$$

The τ_{θ} part is a multi-layer perceptron (MLP), aiming to map the observed data to the input condition $\tau_{\theta}(x_0^c)$. Subsequently, the condition is mapped to the intermediate layers of the backbone network through a cross-attention layer to guide the model during training. Attention layer can be formalized as:

$$Attention(Q, K, V) = softmax\left(\frac{QK^T}{\sqrt{d}}\right) \cdot V \quad (12)$$

$$Q = W_Q \cdot \varphi(x_T^*), K = W_K \cdot \tau_{\theta}(C), V = W_V \cdot \tau_{\theta}(C)$$

where $\varphi(x_T^*)$ denotes a intermediate representation of the backbone network implementing ϵ_{θ} and W_Q, W_K, W_V are learnable projection metrics.

6) *Inference process of mbVDiT*: During the inference phase, we randomly sample complete noise data directly from a standard normal distribution and apply the denoising process. Finally, we decode the new samples from the denoised latent distribution.

7) *Training process and Loss function*: Training mbVDiT involves two stages: (1) pre-training the VAE encoder and decoder; and (2) training the diffusion model in the latent space.

The loss function in the first stage consists of two parts, reconstruction loss and KL divergence respectively. Simultaneously training the encoder and decoder to minimize this loss.

$$\mathcal{L}_{VAE} = \|X - \hat{X}\| + KL(\mathcal{N} \sim (\mu, \sigma^2) \| \mathcal{N}(0, 1)) \quad (13)$$

For the second stage, under the condition of C and imputation targets x_t^* , we proceed to refine ϵ_{θ} by minimizing the ensuing loss function:

$$\mathcal{L}_{DM} = \mathbb{E}_{x_0 \sim q(x_0), \epsilon \sim \mathcal{N}(0, \mathbf{I}), t} \|\epsilon - \epsilon_{\theta}(x_t^*, t | C) \odot M\|_2^2 \quad (14)$$

C. Evaluation metrics

To evaluate the performance of mbVDiT and baseline methods, we used four evaluation metrics on three datasets: Pearson correlation coefficient (PCC), Cosine distance (Cosine), Root Mean Square Error (RMSE), and Mean Absolute Error (MAE).

TABLE I: The list of microbial datasets used in the study includes the three cancer types with the highest number of samples from TCGA.

Datasets	Number of Samples/Microbes		Prepro. Samples/Microbes		Droupout Rate
	#Samples	#Microbes	#Samples	#Microbes	
STAD	530		530		87.61%
COAD	561	1289	561	106	63.20%
HNSC	587		587		79.63%
READ	182	1289	182	106	67.06%
ESCA	248		248		88.99%

III. EXPERIMENTAL RESULTS

A. Dataset and pre-processing

All cancer microbiome datasets with different cancer types were obtained from the TCGA public database [33, 34]. Due to the limited data availability, we selected these microbiome datasets from three different cancer types with relatively larger sample sizes as our experimental datasets including Stomach adenocarcinoma (STAD), Colon adenocarcinoma (COAD) and Head and Neck Squamous Cell Carcinoma (HNSC), specifically, Esophageal carcinoma (ESCA) and Rectum adenocarcinoma (READ) datasets with smaller sample sizes were used for each pre-training, the detailed description of the relevant data is provided in Table I.

For data preprocessing, we first conducted screening on microbial features. To maintain consistency, we then combined the three datasets. Then, microbes with missing data rates (dropout) exceeding 95% were removed. mbVDiT requires data from each sample to be on the same scale, so the next step is to normalize the data.

However, properly normalizing microbial data poses a challenge. We have selected a normalization method from benchmark papers [35, 36]. For each distinct cancer dataset, Given a matrix M , mbVDiT normalizes samples row-wise. The normalized matrix is denoted as $M'_{ij} \in R^{n \times d}$, where $M'_{ij} = 10^2 \frac{M_{ij}}{\sum_{k=1}^d M_{ik}}$. To mitigate the influence of extremely large counts, we applied the logarithmic transformation to the normalized matrix. The log-transformed matrix is denoted as $Y \in R^{n \times d}$, where $Y = \log_{10}(M'_{ij} + 1.0)$.

B. Baseline methods

To evaluate the performance of mbVDiT, we first compared with KNN imputation. Due to the limited methods for imputing microbiome data, we sought high-quality alternatives. Although we reproduced this particular method [36], it ran too long and produced suboptimal results, so we excluded it from the baseline comparison. Additionally, we compared several state-of-the-art imputation methods for single-cell data:

TABLE II: Performance comparison between mbVDiT and baselines on three microbiome datasets (STAD, COAD and HNSC) using four evaluation metrics. The black bold part represents the best performance.

PCC ↑	KNN	DeepImpute [15]	AutoImpute [16]	DCA [17]	CpG [32]	scVI [18]	DeepMicroGen [9]	mbVDiT
STAD	0.232±0.021	0.570±0.067	0.477±0.048	0.505±0.025	0.520±0.049	0.596±0.065	0.588±0.065	0.634±0.032
COAD	0.188±0.033	0.653±0.054	0.639±0.085	0.632±0.062	0.599±0.069	0.667±0.059	0.675±0.049	0.704±0.062
HNSC	0.247±0.038	0.592±0.032	0.550±0.043	0.594±0.056	0.585±0.017	0.559±0.028	0.604±0.061	0.626±0.060
Cosine ↑	KNN	DeepImpute [15]	AutoImpute [16]	DCA [17]	CpG [32]	scVI [18]	DeepMicroGen [9]	mbVDiT
STAD	0.430±0.014	0.773±0.059	0.787±0.027	0.746±0.036	0.746±0.027	0.775±0.072	0.775±0.074	0.806±0.057
COAD	0.241±0.037	0.769±0.057	0.650±0.124	0.724±0.064	0.688±0.062	0.716±0.052	0.772±0.072	0.791±0.080
HNSC	0.357±0.031	0.779±0.044	0.794±0.050	0.789±0.026	0.778±0.015	0.776±0.024	0.786±0.031	0.802±0.062
RMSE ↓	KNN	DeepImpute [15]	AutoImpute [16]	DCA [17]	CpG [32]	scVI [18]	DeepMicroGen [9]	mbVDiT
STAD	3.371±0.124	1.572±0.082	1.521±0.055	1.629±0.044	1.462±0.075	2.478±0.085	1.469±0.049	1.320±0.053
COAD	4.336±0.106	1.211±0.076	1.370±0.070	1.183±0.059	1.127±0.045	2.351±0.057	1.002±0.100	0.934±0.054
HNSC	4.128±0.083	1.258±0.058	1.364±0.049	1.246±0.034	1.169±0.022	2.168±0.077	1.245±0.047	1.155±0.027
MAE ↓	KNN	DeepImpute [15]	AutoImpute [16]	DCA [17]	CpG [32]	scVI [18]	DeepMicroGen [9]	mbVDiT
STAD	3.255±0.095	1.388±0.061	1.186±0.039	1.234±0.047	1.308±0.071	2.221±0.068	1.325±0.058	0.956±0.050
COAD	3.862±0.114	0.804±0.065	0.864±0.128	0.728±0.061	0.739±0.063	2.132±0.049	0.627±0.109	0.530±0.070
HNSC	3.679±0.096	0.986±0.064	0.981±0.045	0.993±0.018	0.906±0.021	0.847±0.083	0.978±0.028	0.807±0.020

- DeepMicroGen [9]: It is a generative adversarial network-based method for longitudinal microbiome data imputation.
- DeepImpute [15]: It is an accurate, fast and scalable deep neural network method to impute single-cell RNA-seq data.
- AutoImpute [16]: It is a autoencoder based method imputation of single-cell RNA-seq data.
- DCA [17]: It is a method for denoising single-cell RNA-seq data using a deep count autoencoder.
- CpG [32]: It is a transformer-based method for imputation of single-cell methylomes.
- scVI [18]: It is deep generative modeling for single-cell transcriptomics.

The detailed results are presented in Table II.

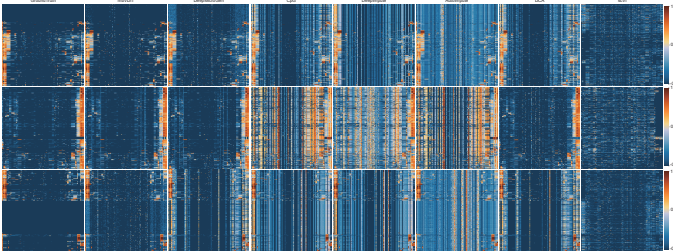


Fig. 2: Visualization of the imputation performance of various baseline methods.

C. mbVDiT improves the accuracy of imputed data

To further demonstrate the superior performance of our method compared to other state-of-the-art methods, we visualize the imputed microbiome data for each method (Fig. 2). The closer the predicted heatmap is to the ground truth, the higher the prediction accuracy. We splice the mask part to form the real label, and we apply the same method to the imputation results of each baseline method.

We normalized both the actual expression matrix and the imputed matrix. To enhance the visualization, we used hi-

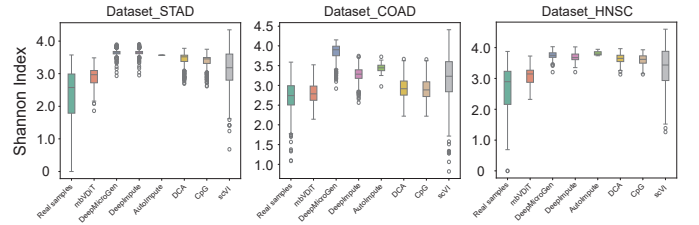


Fig. 3: Comparison of alpha-diversity based on Shannon index measured from real data and the imputed data by different methods.

erarchical clustering to sort the microbes, ensuring that the expression matrix exhibits pattern-like features.

From the figure (Fig. 2), it is evident that the hierarchical clustering diagram obtained using our method for data imputation shows the most distinct hierarchy and the data patterns are closest to the real data patterns. This further demonstrates that our method provides the best imputation results and effectively preserves the original data distribution.

D. mbVDiT preserves the similar characteristics of missing samples in data imputation

To further validate the performance of methods, we conducted an alpha-diversity analysis on the imputed microbiome data. Firstly, we calculate the relative abundance of each species for each sample, and then we calculated the alpha-diversity using the Shannon index for both the real samples and the imputed data, and a box plot of alpha diversity was also plotted (Fig. 3). We masked 30% of the original data and performed imputation on this basis, then calculated the alpha-diversity values of the imputed data.

We observed that the alpha diversity box plot calculated from the imputed data using our method is the closest to that of the original data, while other methods show relatively larger deviations. Our proposed method better preserves the community distribution characteristics and species abundance of the original data after imputing missing values. The microbial

diversity after imputation closely matches the real data for each cancer type.

E. mbVDiT retains the Pearson correlation coefficients of imputed data

To further validate the superior performance of our model. Here, we calculated the Pearson correlation coefficients for imputed data. First, we calculated the PCCs between each pair of microbes in the imputed microbiome matrices for each method. After obtaining the correlation coefficient matrices, we applied hierarchical clustering to sort the matrices, enhancing the visualization effect (Fig. 4).

It can be observed that our method preserves microbial distribution characteristics similar to real samples after imputation. Among the baseline methods, DeepMicroGen has the best visualization effect, and its visualization effect of PCCs between microbes is very similar to our method. However, in some details, our method performs better than the DeepMicroGen.

F. mbVDiT preserves the Pearson correlation coefficients between real data and imputed data for microbe-to-microbe

To further validate the superior performance of our model. In this section, we calculated the Pearson correlation coefficients between each microbe in the imputed microbiome matrix for each method and the corresponding microbe in the actual expression matrix. After obtaining the correlation coefficient matrix, we sorted the PCC values for each microbe in descending order according to the mbVDiT method, and subsequent methods followed this order.

From the heatmap in section A of the figure (Fig. 5), it can be seen that our method better preserves the original data distribution characteristics of each microbe after imputation compared to other methods. To facilitate a better visual comparison, we plotted a corresponding box plot using these PCC values (Fig. 5). From section B of the figure, it can be further seen that our method generally outperforms the other methods.

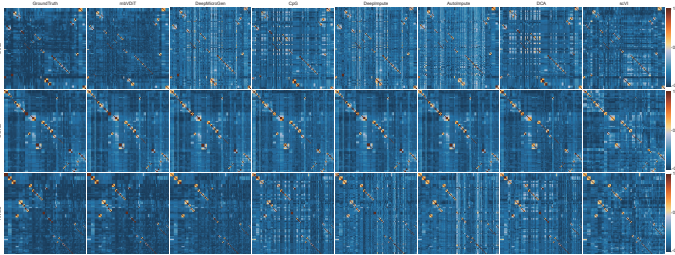


Fig. 4: Visualization of Pearson correlation coefficients for imputed data between microbe and microbe.

G. mbVDiT improves robustness in highly sparse microbiome data

In microbiome data studies, the rate of missing data in patients with different cancer types may vary due to various reasons [37]. Data sparsity is defined as the percentage of zero elements in the expression matrix. To investigate the impact

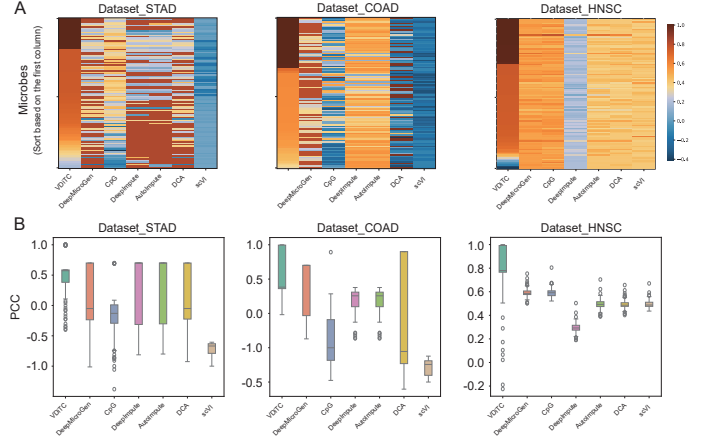


Fig. 5: (A) Heatmap of Pearson correlation coefficients between imputed and real microbiome data. (B) Box plot of Pearson correlation coefficients between imputed microbiome data and real microbiome data.

of different masking ratios on model performance, we applied three different masking ratios to the non-zero elements based on the original missing rate: 10%, 30%, and 50%. Our method masks data in two stages: once on the original input data and again on the intermediate latent representation. In this, varying mask ratios are applied during the masking phase of the original input data, while the masking ratio in the second phase for the latent space is fixed at 30%. Experimental results show that in our proposed method, different masking ratios have minimal impact on the results, further indicating that our method possesses strong stability (Table VI).

H. Ablation studies

We conduct ablation experiment to verify the modules of mbVDiT in these aspects: (1) Different backbone networks; (2) Whether to include metadata as condition; (3) Whether to pre-training VAE.

1) *Different backbone networks*: In our model, the backbone network employs DiT Blocks, which are based on cross-attention mechanism. The purpose is to leverage the cross-attention mechanism to fuse different types of conditions, enabling the model to better generate new data. To validate the effectiveness of the cross-attention mechanism, we compared our method with the popular Unet network.

The experimental results indicate that a backbone network predominantly based on attention mechanisms is more suitable for our specific task (Table III).

2) *Whether to include metadata as condition*: In the field of bioinformatics, each dataset contains a wealth of information. In our method, we utilize various metadata from patients. To validate the effectiveness of this data, we conducted ablation experiments.

Experimental data indicate that adding metadata to enrich the conditions of the diffusion model had slight improvement in four metrics. In conclusion, the experimental results also demonstrate that integrating various metadata to enrich

TABLE III: Ablation experiments on different backbone networks.

PCC \uparrow	STAD	COAD	HNSC
Backbone w/ Unet	0.523 \pm 0.037	0.597 \pm 0.066	0.538 \pm 0.011
Backbone w/ DiT	0.634\pm0.032	0.704\pm0.062	0.626\pm0.060
Cosine \uparrow	STAD	COAD	HNSC
Backbone w/ Unet	0.755 \pm 0.021	0.722 \pm 0.013	0.716 \pm 0.009
Backbone w/ DiT	0.806\pm0.057	0.791\pm0.080	0.802\pm0.062
RMSE \downarrow	STAD	COAD	HNSC
Backbone w/ Unet	1.429 \pm 0.058	1.238 \pm 0.038	1.246 \pm 0.050
Backbone w/ DiT	1.32\pm0.053	0.934\pm0.054	1.155\pm0.027
MAE \downarrow	STAD	COAD	HNSC
Backbone w/ Unet	1.244 \pm 0.045	0.744 \pm 0.060	0.933 \pm 0.021
Backbone w/ DiT	0.956\pm0.050	0.530\pm0.070	0.807\pm0.020

conditions is effective, providing insights and assistance for subsequent experiments (Table IV). This is a worthwhile area for further investigation. Our experiments directly validate that integrating various types of metadata is beneficial for deep learning models.

TABLE IV: Ablation experiments on whether the proposed mbVDiT with the condition (metadata).

PCC \uparrow	STAD	COAD	HNSC
w/o Metadata	0.619 \pm 0.011	0.691 \pm 0.076	0.592 \pm 0.020
w/ Metadata	0.634\pm0.032	0.704\pm0.062	0.626\pm0.060
Cosine \uparrow	STAD	COAD	HNSC
w/o Metadata	0.786 \pm 0.013	0.779 \pm 0.070	0.786 \pm 0.017
w/ Metadata	0.806\pm0.057	0.791\pm0.080	0.802\pm0.062
RMSE \downarrow	STAD	COAD	HNSC
w/o Metadata	1.331 \pm 0.060	0.963 \pm 0.054	1.173 \pm 0.032
w/ Metadata	1.320\pm0.053	0.934\pm0.054	1.155\pm0.027
MAE \downarrow	STAD	COAD	HNSC
w/o Metadata	0.963 \pm 0.057	0.557 \pm 0.082	0.828 \pm 0.038
w/ Metadata	0.956\pm0.050	0.530\pm0.070	0.807\pm0.020

3) *Whether to pre-train VAE*: Due to the limited amount of data in individual cancer datasets, training on a single dataset cannot achieve the expected results for the model. Therefore, we use pre-training method to improve model performance. By leveraging datasets from other types of cancers, we learn a shared weight matrix and transfer this matrix to the VAE module in mbVDiT as initial weights. In order to verify that pre-training can improve our model performance, we conducted comparative experiments on the VAE module of mbVDiT.

The results (Table V) showed that using pre-training significantly improved the performance of the model. This also proves that pre-training can effectively address the objective factor of a small sample size in the datasets.

TABLE V: Ablation experiments on whether pre-training VAE module.

PCC \uparrow	STAD	COAD	HNSC
w/o Pre_train	0.518 \pm 0.011	0.613 \pm 0.065	0.589 \pm 0.014
w/ Pre_train	0.634\pm0.032	0.704\pm0.062	0.626\pm0.060
Cosine \uparrow	STAD	COAD	HNSC
w/o Pre_train	0.648 \pm 0.009	0.737 \pm 0.040	0.741 \pm 0.013
w/ Pre_train	0.806\pm0.057	0.791\pm0.080	0.802\pm0.062
RMSE \downarrow	STAD	COAD	HNSC
w/o Pre_train	1.442 \pm 0.013	0.996 \pm 0.015	1.276 \pm 0.026
w/ Pre_train	1.32\pm0.053	0.934\pm0.054	1.155\pm0.027
MAE \downarrow	STAD	COAD	HNSC
w/o Pre_train	1.045 \pm 0.014	0.561 \pm 0.011	0.870 \pm 0.010
w/ Pre_train	0.956\pm0.050	0.530\pm0.070	0.807\pm0.020

TABLE VI: Robustness experiments of model performance under different masked ratios.

Rate	PCC \uparrow			Cosine \uparrow		
	10%	30%	50%	10%	30%	50%
STAD	0.619 \pm 0.010	0.634 \pm 0.032	0.609 \pm 0.016	0.794 \pm 0.006	0.806 \pm 0.057	0.787 \pm 0.019
COAD	0.693 \pm 0.010	0.704 \pm 0.062	0.703 \pm 0.065	0.791 \pm 0.007	0.791 \pm 0.080	0.796 \pm 0.049
HNSC	0.628 \pm 0.019	0.626 \pm 0.060	0.613 \pm 0.007	0.793 \pm 0.026	0.802 \pm 0.062	0.796 \pm 0.036
Rate	RMSE \downarrow			MAE \downarrow		
	10%	30%	50%	10%	30%	50%
STAD	1.273 \pm 0.029	1.320 \pm 0.053	1.306 \pm 0.065	0.910 \pm 0.019	0.956 \pm 0.050	0.935 \pm 0.067
COAD	0.868 \pm 0.050	0.934 \pm 0.054	0.937 \pm 0.049	0.507 \pm 0.008	0.530 \pm 0.070	0.526 \pm 0.039
HNSC	1.159 \pm 0.028	1.155 \pm 0.027	1.161 \pm 0.024	0.812 \pm 0.021	0.807 \pm 0.020	0.816 \pm 0.003

IV. CONCLUSIONS

In this paper, we proposed a masked conditional diffusion model with variational autoencoder (mbVDiT) for microbiome data denoising and imputation. By masking part of the latent representation and utilizing the remaining portion and patient metadata as condition, the diffusion model becomes well-guided and controllable throughout the reverse process. In addition, mbVDiT uses a VAE-based pre-trained model to integrate other public microbiome datasets to enhance its performance. Experiments on three TCGA microbiome data showed that our approach achieves the best overall performance compared to other baseline methods.

ACKNOWLEDGMENT

The work was supported in part by the National Natural Science Foundation of China (62262069), in part by the Yunnan Fundamental Research Projects under Grants (202201AT070469) and the Yunnan Talent Development Program - Youth Talent Project.

REFERENCES

- [1] V. Gopalakrishnan, C. N. Spencer *et al.*, "Gut microbiome modulates response to anti-pd-1 immunotherapy in melanoma patients," *Science*, vol. 359, no. 6371, pp. 97–103, 2018.
- [2] C. Jin, G. K. Lagoudas, C. Zhao, S. Bullman, A. Bhutkar, B. Hu, S. Ameh, D. Sandel, X. S. Liang, S. Mazzilli *et al.*, "Commensal microbiota promote lung cancer development via $\gamma\delta$ T cells," *Cell*, vol. 176, no. 5, pp. 998–1013, 2019.

- [3] C. Ma, M. Han *et al.*, “Gut microbiome-mediated bile acid metabolism regulates liver cancer via nkt cells,” *Science*, vol. 360, no. 6391, pp. 858–859, 2018.
- [4] A. Gihawi, Y. Ge, J. Lu, D. Puiu, A. Xu, C. S. Cooper, D. S. Brewer, M. Perteu, and S. L. Salzberg, “Major data analysis errors invalidate cancer microbiome findings,” *MBio*, vol. 14, no. 5, pp. e01607–23, 2023.
- [5] M. L. Calle, “Statistical analysis of metagenomics data,” *Genomics and Informatics*, vol. 17, no. 1, 2019.
- [6] J. Yu, Q. Feng, S. H. Wong, D. Zhang, Q. yi Liang, Y. Qin, L. Tang, H. Zhao, J. Stenvang, Y. Li *et al.*, “Metagenomic analysis of faecal microbiome as a tool towards targeted non-invasive biomarkers for colorectal cancer,” *Gut*, vol. 66, no. 1, pp. 70–78, 2017.
- [7] H. Li, “Microbiome, metagenomics, and high-dimensional compositional data analysis,” *Annual Review of Statistics and Its Application*, vol. 2, pp. 73–94, 2015.
- [8] M. Calgario, C. Romualdi, L. Waldron, D. Risso, and N. Vitulo, “Assessment of single cell rna-seq statistical methods on microbiome data,” *Genome Biology*, vol. 21, no. 1, p. 191, 2020.
- [9] J. M. Choi, M. Ji, L. T. Watson, and L. Zhang, “Deepmicrogen: a generative adversarial network-based method for longitudinal microbiome data imputation,” *Bioinformatics*, vol. 39, no. 5, p. btad286, 2023.
- [10] Z. Huang, J. Wang, X. Lu, A. Mohd Zain, and G. Yu, “scggan: single-cell rna-seq imputation by graph-based generative adversarial network,” *Briefings in Bioinformatics*, vol. 24, no. 2, p. bbad040, 2023.
- [11] G. Gaziv, R. Belyi, N. Granot, A. Hoogi, F. Strappini, T. Golan, and M. Irani, “Self-supervised natural image reconstruction and large-scale semantic classification from brain activity,” *NeuroImage*, vol. 254, p. 119121, 2022.
- [12] Y. Song, P. Dhariwal, M. Chen, and I. Sutskever, “Consistency models,” *arXiv preprint arXiv:2303.01469*, 2023.
- [13] V. Rulloni, O. Bustos, and A. G. Flesia, “Large gap imputation in remote sensed imagery of the environment,” *Computational Statistics and Data Analysis*, vol. 56, no. 8, pp. 2388–2403, 2012.
- [14] J. Ernst and M. Kellis, “Large-scale imputation of epigenomic datasets for systematic annotation of diverse human tissues,” *Nature Biotechnology*, vol. 33, no. 4, pp. 364–376, 2015.
- [15] C. Arisdakessian, O. Poirion, B. Yunits, X. Zhu, and L. X. Garmire, “Deepimpute: an accurate, fast, and scalable deep neural network method to impute single-cell rna-seq data,” *Genome Biology*, vol. 20, pp. 1–14, 2019.
- [16] D. Talwar, A. Mongia, D. Sengupta, and A. Majumdar, “Autoimpute: Autoencoder based imputation of single-cell rna-seq data,” *Scientific Reports*, vol. 8, no. 1, p. 16329, 2018.
- [17] G. Eraslan, L. M. Simon, M. Mircea, N. S. Mueller, and F. J. Theis, “Single-cell rna-seq denoising using a deep count autoencoder,” *Nature Communications*, vol. 10, no. 1, p. 390, 2019.
- [18] R. Lopez, J. Regier, M. B. Cole, M. I. Jordan, and N. Yosef, “Deep generative modeling for single-cell transcriptomics,” *Nature Methods*, vol. 15, no. 12, pp. 1053–1058, 2018.
- [19] L. Yang, Z. Zhang, Y. Song, S. Hong, R. Xu, Y. Zhao, W. Zhang, B. Cui, and M.-H. Yang, “Diffusion models: A comprehensive survey of methods and applications,” *ACM Computing Surveys*, vol. 56, no. 4, pp. 1–39, 2023.
- [20] X. Wang, H. Zhang *et al.*, “An observed value consistent diffusion model for imputing missing values in multivariate time series,” in *Proceedings of the 29th ACM SIGKDD*, 2023, pp. 2409–2418.
- [21] X. Li, W. Min, S. Wang, C. Wang, and T. Xu, “stMCDI: Masked Conditional Diffusion Model with Graph Neural Network for Spatial Transcriptomics Data Imputation,” *arXiv:2403.10863*, 2024.
- [22] X. Li, F. Zhu, and W. Min, “SpaDiT: Diffusion Transformer for Spatial Gene Expression Prediction using scRNA-seq,” *arXiv:2407.13182*, 2024.
- [23] J. Ho, A. Jain, and P. Abbeel, “Denoising diffusion probabilistic models,” *Advances in Neural Information Processing Systems*, vol. 33, pp. 6840–6851, 2020.
- [24] Y. Song, J. Sohl-Dickstein, D. P. Kingma, A. Kumar, S. Ermon, and B. Poole, “Score-based generative modeling through stochastic differential equations,” in *International Conference on Learning Representations (ICLR)*, 2021. [Online]. Available: <https://arxiv.org/abs/2011.13456>
- [25] R. Rombach, A. Blattmann, D. Lorenz, P. Esser, and B. Ommer, “High-resolution image synthesis with latent diffusion models,” in *Proceedings of the IEEE/CVF Conference on Computer Vision and Pattern Recognition*, 2022, pp. 10684–10695.
- [26] K. He, X. Chen, S. Xie, Y. Li, P. Dollár, and R. Girshick, “Masked autoencoders are scalable vision learners,” in *Proceedings of the IEEE/CVF Conference on Computer Vision and Pattern Recognition*, 2022, pp. 16000–16009.
- [27] Z. Hou, X. Liu, Y. Cen, Y. Dong, H. Yang, C. Wang, and J. Tang, “Graphmae: Self-supervised masked graph autoencoders,” in *Proceedings of the 28th ACM SIGKDD Conference on Knowledge Discovery and Data Mining*, 2022, pp. 594–604.
- [28] J. Sohl-Dickstein, E. Weiss, N. Maheswaranathan, and S. Ganguli, “Deep unsupervised learning using nonequilibrium thermodynamics,” in *International Conference on Machine Learning*. PMLR, 2015, pp. 2256–2265.
- [29] Y. Takagi and S. Nishimoto, “High-resolution image reconstruction with latent diffusion models from human brain activity,” in *Proceedings of the IEEE/CVF Conference on Computer Vision and Pattern Recognition*, 2023, pp. 14453–14463.
- [30] G. Kim, T. Kwon, and J. C. Ye, “Diffusionclip: Text-guided diffusion models for robust image manipulation,” in *Proceedings of the IEEE/CVF Conference on Computer Vision and Pattern Recognition*, 2022, pp. 2426–2435.
- [31] J. Ho and T. Salimans, “Classifier-free diffusion guidance,” *arXiv preprint arXiv:2207.12598*, 2022.
- [32] G. De Waele, J. Clauwaert, G. Menschaert, and W. Waegeman, “Cpg transformer for imputation of single-cell methylomes,” *Bioinformatics*, vol. 38, no. 3, pp. 597–603, 2022.
- [33] C. J. C. Kyle Chang *et al.*, “The cancer genome atlas pan-cancer analysis project,” *Nature Genetics*, vol. 45, no. 10, pp. 1113–1120, 2013.
- [34] A. B. Dohlman, D. A. Mendoza, S. Ding, M. Gao, H. Dressman, I. D. Iliev, S. M. Lipkin, and X. Shen, “The cancer microbiome atlas: a pan-cancer comparative analysis to distinguish tissue-resident microbiota from contaminants,” *Cell host & microbe*, vol. 29, no. 2, pp. 281–298, 2021.
- [35] M. Cappellato, G. Baruzzo, and B. Di Camillo, “Investigating differential abundance methods in microbiome data: A benchmark study,” *PLoS Computational Biology*, vol. 18, no. 9, p. e1010467, 2022.
- [36] R. Jiang, W. V. Li, and J. J. Li, “mbimpute: an accurate and robust imputation method for microbiome data,” *Genome Biology*, vol. 22, no. 1, p. 192, 2021.
- [37] J. W. Graham, P. E. Cumsille, and E. Elek-Fisk, “Methods for handling missing data,” *Handbook of Psychology*, pp. 87–114, 2013.